Fission fragment properties in fast-neutron-induced fission of ^{237}Np

A. A. Naqvi,* F. Käppeler, and F. Dickmann
Kernforschungszentrum Karlsruhe GmbH, Institut für Kernphysik, D-7500 Karlsruhe, Federal Republic of Germany

R. Müller†
Universität Tübingen, Physikalisches Institut, D-7400 Tübingen, Federal Republic of Germany
(Received 16 October 1985)

We report on a four-parameter measurement of the kinetic energies E and the velocities v of correlated fragments in fast-neutron-induced fission of ^{237}Np. The influence of excitation energy on the important fragment properties such as mass, kinetic energy, and prompt neutron emission have been investigated experimentally at 0.80 and 5.55 MeV neutron energy. Our results include mean values of fragment properties before and after neutron evaporation, e.g., of fragment velocities and masses, total kinetic energies, and the respective variances. Also given are the distributions of fragment mass, of $E_{k,\mathrm{tot}}$, the variance of $E_{k,\mathrm{tot}}$, as well as the number of prompt fission neutrons as a function of fragment mass. These results show that shell effects are strong near threshold at $E_n = 0.80$ MeV, but decrease significantly at the higher excitation energy, in qualitative agreement with the model of Wilkins, Chasman, and Steinberg. However, the observed increase in the number of prompt fission neutrons, which appears only in the heavy fragment, cannot be explained by this model.

I. INTRODUCTION

The results presented in this paper complement a previous study,[1] where we investigated the behavior of fission fragment properties from fast neutron induced fission on ^{235}U at different excitation energies. Both experiments are precise $(2E,2v)$ measurements of the kinetic energies, E, and velocities, v, of correlated fragments. Data of this type provide information on the role of pairing and shell effects in the fission process, and—if taken at different excitation energies—on fission dynamics.

^{237}Np is of general interest because it represents a fissioning system which differs from ^{235}U in two respects: (i) ^{238}Np is an odd-odd system compared to the even-even ^{236}U, and hence one would expect a reduced influence of pairing effects. (ii) The fission threshold of ^{237}Np at 0.7 MeV neutron energy allows for investigations close to the barrier, whereas the fission threshold of ^{235}U is 0.7 MeV below the neutron separation energy.

Because of the experimental difficulty of multiparameter measurements on correlated fission fragments, the two previous investigations on ^{237}Np were restricted to the fragment kinetic energies. The measurement of Kuzminov, Sergachev, and Smirenkina[2] in the neutron energy range from 0.7 to 5.4 MeV suffered from limited resolution. The only other work by Ashgar *et al.*[3] was performed at thermal neutron energy, i.e., 0.7 MeV below the fission barrier.

Our measurements were carried out at two neutron energies, 0.8 and 5.5 MeV, corresponding to excitation energies in the compound system of 0.1 and 4.8 MeV. In this way, information is obtained close to the threshold and at the maximum excitation before the onset of second chance fission. The technique of our measurement was already described in detail.[1,4] Therefore, only a brief outline is given in Sec. II together with the characteristic features of the ^{237}Np targets. The results are presented in Sec. III and are discussed in Sec. IV.

II. EXPERIMENT AND DATA ANALYSIS

Both experiment and data analysis were identical to our previous experiment on ^{235}U (Ref. 1) and therefore only a brief discussion is presented here. Any details may be found in Ref. 1.

A schematic view of the experimental setup is shown in Fig. 1. Neutrons are produced via the ^{7}Li(p,n) and the ^{2}H(d,n) reactions. The charged particle beam from the Karlsruhe 3.75 MV Van de Graaff accelerator was pulsed to about 700 ps and therefore beam pickup signals could be used directly for the neutron time-of-flight (TOF) determination instead of time zero detectors. The sample was a 100 μg/cm^2 thick layer of NpO_2 evaporated onto a 30 μg/cm^2 thick carbon backing. The sample material was enriched in ^{237}Np to 99.52% with negligible amounts

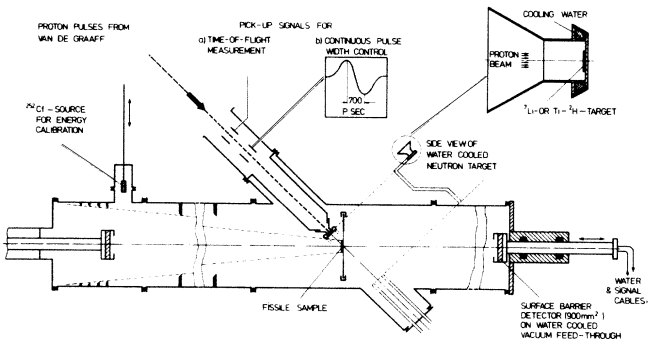

FIG. 1. Schematic view of the experimental setup.

of other elements (0.1% U, 0.081% ^{238}Pu, 0.015% ^{239}Pu, 0.002% ^{240}Pu, and 0.02% Th). Large area silicon surface barrier detectors (Ortec AF-90-900-60), which were calibrated by ^{252}Cf sources, were used to detect the fragments. Various collimators in the flight tube shielded the detectors from fragments scattered from the walls. Typical fission rates were 100 s^{-1}.

For investigation of systematic uncertainties in the determination of the time zero point t_0 in the TOF spectra, measurements were performed at four different fragment flight paths of 70, 170, 270, and 375 mm. Accurately calibrated distance pieces guaranteed flight path uncertainties of only 0.05 mm. From the runs at the two short flight paths, which were carried out at least once a day, the time zero point of the TOF spectra was determined. To reduce the effects of long term drifts in electronics, detectors, and the accelerator on the evaluated data, the measurements were subdivided in 34 runs at 70 mm, 18 runs at 170 mm, 9 runs at 270 mm, and 15 runs at 375 mm. For each flight path 10^4 fission events were registered at each neutron energy. In between those runs, 42 time calibrations and 29 energy calibrations were carried out. An example for the directly measured raw data is given in Fig. 2, showing the TOF spectra at the various flight paths. For better readability the original resolution had been reduced by summation over four neighboring channels.

Fission events were recorded in list mode on magnetic tape. For a continuous control throughout the measurements, TOF and pulse height spectra were generated on line for each of the detectors.

Data analysis is based on momentum and mass conservation of the fissioning system of mass A_c. The primary fragments $A^*_{1,2}$ are emitted under 180° with velocities $v^*_{1,2}$, where the asterisk denotes primary quantities before neutron evaporation. One obtains, for the primary fragment masses and kinetic energies,

$$A^*_{1,2}=\frac{v^*_{1,2}}{v^*_1+v^*_2}A_c \ , \tag{1}$$

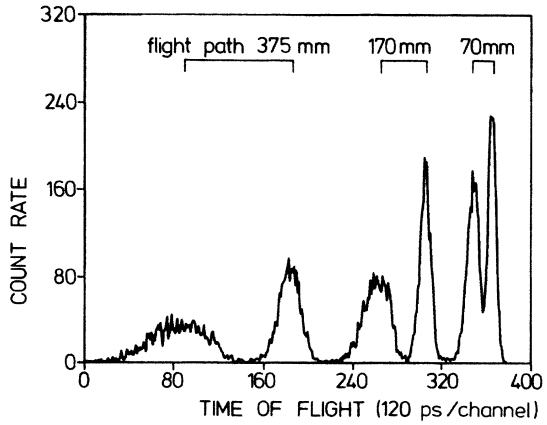

FIG. 2. Time-of-flight spectra taken at various flight paths. For better readability, the spectra are compressed by a factor 4.

$$E^*_{1,2}=\frac{A^*_{1,2}}{2}v^{*2}_{1,2} \ , \tag{2}$$

$$E^*_{k,\mathrm{tot}}=E^*_1+E^*_2=\frac{A_c}{2}v^*_1v^*_2 \ . \tag{3}$$

The velocities of the primary fragments, $v^*_{1,2}$, cannot be measured because the fragments evaporate neutrons within $\leq 10^{-14}$ s. However, if one assumes that neutrons are emitted from fully accelerated fragments with forward/backward symmetry ($\cos\theta=0$), there is no change of velocity on the average: $v_i^*=v_i$. Then, the fragment masses after neutron emission follow immediately from the measured kinetic energies:

$$A_{1,2}=\frac{2E_{1,2}}{v^2_{1,2}} \ . \tag{4}$$

Finally, the number of neutrons emitted as a function of fragment mass is

$$\nu(A^*_{1,2})=\frac{A^*_{1,2}-A_{1,2}}{m_{\mathrm{n}}} \ , \tag{5}$$

with m_{n} being the neutron mass.

It is obvious from Eqs. (1)–(5) that the velocity determination is the crucial point in this experiment and therefore great care was devoted to the measurement of this quantity, including frequent internal calibrations, measurements at different flight paths, and detailed checks for short and long term stability in all important parameters.

The various steps of data analysis were as follows.

(i) Determination of time zero $t_0=t_0(E,A)$ considering the specific timing properties of the detectors with respect to E and A.

(ii) Corrections for the momentum of the incoming neutron and the fragment energy loss in the sample.

(iii) Critical selection of data to eliminate background events mainly due to fission by scattered neutrons which appear delayed with respect to the time zero point. About 2% of all events fell into this category and were rejected.

(iv) For each single run, and for light and heavy fragments separately, we calculated mean values, rms widths σ, and correlation coefficients r of all relevant observables in order to check the stability and assess the uncertainties of the data. Then, the mean values, variances, covariances of the primary (v^*,A^*,E^*) and secondary quantities (A,E), and of the number of prompt fission neutrons, ν, were calculated from the data taken at 270 and 375 mm flight paths using the ($2E,2v$) method. As a check, $E_{k,\mathrm{tot}}$ was also determined by the ($2E$) method,[5] but with revised calibration constants as derived in our previous work on ^{235}U (Ref. 1). These results were summarized to yield the primary distributions $P(A^*)$, $P(v^*)$, $P(A^*_H,E^*_{k,\mathrm{tot}})$, and the functions $E^*_{k\mathrm{tot}}(A^*_H)$, $\sigma_{E^*_{k,\mathrm{tot}}}(A^*_H)$, $\nu(A^*)$, and $\sigma_\nu(A^*)$.

(v) Final corrections to these results were applied for resolution effects and for geometric effects (flight path differences for extreme tracks between sample and detector, deviation from collinearity).

The systematic uncertainties of the results are discussed in detail in Ref. 1 and are of order 200 keV for $E^*_{k,\mathrm{tot}}$ and 0.06 mass units for A^*_H. As the systematic uncertainties

are identical for all measurements, they can be neglected in the comparison of the results obtained at the two different neutron energies.

III. RESULTS

Numerical values of all results presented here can be found elsewhere.[6]

A. Kinetic energies and velocities

The kinetic energies of the light fragments are significantly affected by the excitation energy of the fissioning system. This becomes evident from the comparison of the mean values E_k^* and $\sigma_{E_k^*}$ at both neutron energies. The mean kinetic energy of the heavy fragments remains constant while that of the light fragments decreases from 101.78±0.18 MeV to 101.03±0.20 MeV. The corresponding gradient $\Delta E_{k,\mathrm{tot}}/\Delta E_{\mathrm{exc}} = -0.20\pm0.008$ appears to be in good agreement with the value −0.28 reported by Kuzminov *et al.*[2]

The present results for ^{237}Np at $E_n = 0.8$ MeV can also be compared with those of Andritsopoulos[7] for thermal neutron induced fission of ^{235}U, because the excitation energies in both compound systems are nearly identical. Hence, one may expect similar trends in the results. If the total kinetic energy $E_{k,\mathrm{tot}}^*$ given by Andritsopoulos is extrapolated to $Z=93$ using the empirical relation of Unik *et al.*,[8] one obtains $E_{k,\mathrm{tot}} = 174.3$ MeV, in good agreement with the 174.00±0.28 MeV determined in this experiment.

B. Mass distribution

Comparison of the mean masses of the light and heavy fragments with the corresponding values of Andritsopoulos[7] in Table I shows that the mean heavy fragment mass is practically unchanged and that the increase in the mass of the compound nucleus is carried away by the light fragment alone. According to Wilkins, Steinberg, and Chasman,[9] the mean mass of the heavy fragments is stabilized by their near doubly magic configuration. Hence, an increase in the mass of the compound system leads to a corresponding increase in the mean mass of the light fragments.

With increasing excitation energy, there are significant changes in the mass distribution. Figure 3 shows that the symmetrical component in the mass distribution is strongly enhanced and that the fine structure is damped out, both indicating the weakening of shell effects. In addition, the distribution at $E_n = 5.5$ MeV is broadened by the increased neutron emission.

TABLE I. Comparison of the mean number of prompt fission neutrons obtained in this work with previous measurements.

Neutron energy (MeV)	Veeser[a]	Fréhaut *et al.*[b]	This work
0.8	2.73±0.05	2.71	2.73±0.45
5.5	3.46±0.07	3.37	3.43±0.5

[a]Reference 11.
[b]Reference 12.

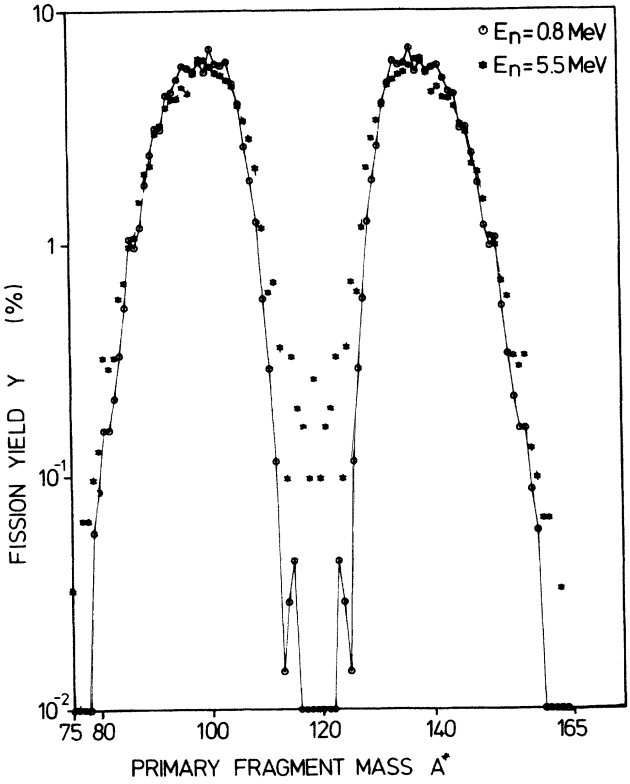

FIG. 3. Yield of primary fission fragment masses for $E_n = 0.8$ and 5.5 MeV.

The peak-to-valley ratio P/V of the mass distribution at 0.80 MeV is difficult to estimate because of poor statistics in the valley region. Depending on the width of the valley (±4 or ±6 mass units) the ratio P/V is either undefined or lies somewhere between 450 and 650. As this spread corresponds roughly to the statistical uncertainty, one obtains, in first approximation, $P/V = 650\pm200$. At the higher neutron energy of 5.5 MeV, this value has reduced to $P/V = 30\pm5$. These results are in good agreement with radiochemical measurements of Borisova *et al.*,[10] who determined the P/V ratio from the yield of ^{115}Cd relative to the mean of the ^{99}Mo and ^{140}Ba yields. For $E_n = 0.8$ and 4.15 MeV these authors reported ratios of 670±70 and 70±7. With an empirical relation derived by Borisova *et al.* on the basis of their experimental data, one would expect an extrapolated value of $P/V = 26$ for $E_n = 5.5$ MeV. From their $2E$ experiment at $E_n = 5.4$ MeV Kuzminov *et al.*[2] obtained a ratio $P/V = 34\pm3$.

The fine structure in the primary mass distribution can best be seen from the linear plot in Fig. 4, where it is emphasized by the solid line. It is prominent for the masses 134, 137, 139, 142, 144, and 147. This period is due to pairing effects, which favor fragments with even proton numbers (also see Sec. IV).

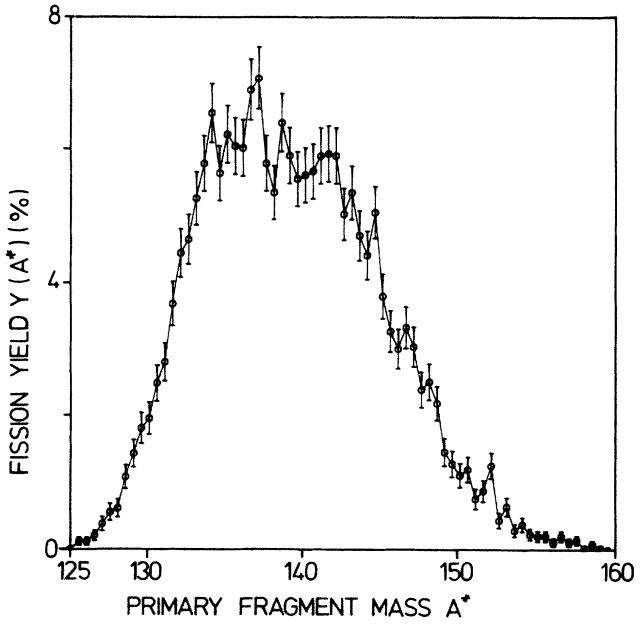

FIG. 4. Yield of primary fission fragment masses for $E_n = 0.8$ MeV in steps of 0.5 mass units (linear scale).

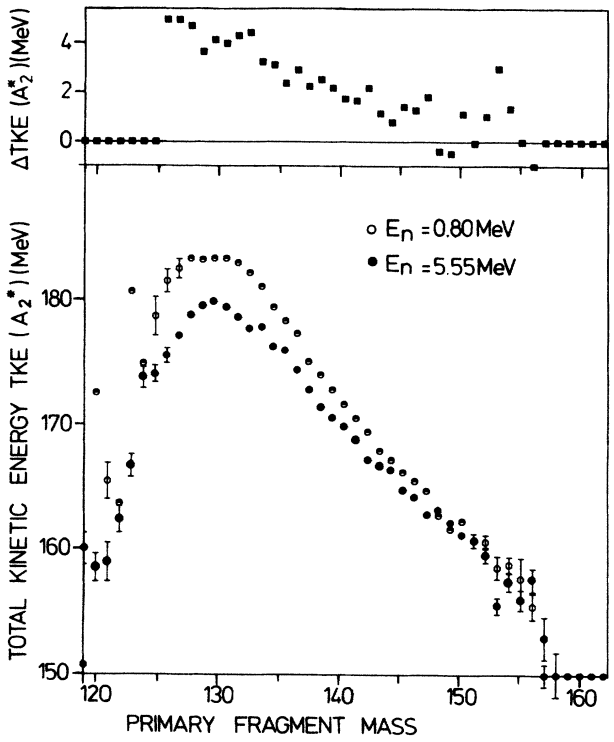

FIG. 5. Distribution of total kinetic energy $E_{k,\mathrm{tot}}$ as a function of primary fragment mass for $E_n = 0.8$ and 5.5 MeV.

C. Total kinetic energy versus primary mass

Most of the kinetic energy is due to Coulomb repulsion between the two fragments and is approximately

$$E_{k,\mathrm{tot}} \simeq E_{\mathrm{Coul}} = \frac{e^2 Z_L Z_H}{D} ,$$

where eZ_L and eZ_H are the electric charges of the light and heavy fragments. Hence, $E_{k,\mathrm{tot}}$ is mainly determined by the deformation of the fragments. For small deformations (e.g., $A_H = 132$) their scission point distance D is small, leading to a maximum of $E_{k,\mathrm{tot}}$, as is evident from Fig. 5. For symmetric fission the large deformations lead to a reduction of the total kinetic energy by 10–15 MeV. The higher excitation at $E_n = 5.5$ MeV results in a decrease of $E_{k,\mathrm{tot}}$ by 2–3 MeV for the magic fragments, probably due to additional deformation as a consequence of weakened shell effects. Obviously, the gradient $\Delta E_{k,\mathrm{tot}}/\Delta E_{\mathrm{exc}}$ is significantly larger for the magic fragments (-0.7) compared to that for the mean values (-0.2). For fragment masses above $A \simeq 140$ the excitation energy has no effect on $E_{k,\mathrm{tot}}$. The continuous decrease in this region is determined by fragment deformation and by the increasingly asymmetric product ($Z_L Z_H$).

D. Neutron emission

The mean numbers of prompt fission neutrons from this experiment agree very well with direct measurements by Veeser[11] and by Fréhaut *et al.*[12] using large liquid scintillator tanks (see Table I). The relative contributions of the light and heavy fragments to ν_{tot} vary with excitation energy. At $E_n = 0.8$ MeV the ratio is $\nu_L/\nu_H = 1.37$ but decreases to 0.98 at $E_n = 5.5$ MeV, an indication that the higher excitation energy of the compound nucleus goes almost completely into the internal excitation of the heavy fragment. This behavior is very similar to the respective ratios of 1.41 and 0.87 which were obtained for the compound system $^{235}\mathrm{U} + \mathrm{n}$ at somewhat higher excitation ($E_n = 0.5$ and 5.5 MeV).[1]

In Fig. 6 the number of prompt fission neutrons, which is a measure of the internal excitation of the fragments, is plotted versus primary fragment mass, showing the typical "sawtooth" shape. If one assumes an average neutron separation energy of about 6 MeV and an additional neutron kinetic energy of 2 MeV, it requires 8 MeV excitation energy to evaporate one neutron. In the upper part of Fig. 6, the difference in the $\nu(A)$ distributions for $E_n = 0.8$ and 5.5 MeV is shown on an enlarged scale. It confirms clearly that the increase in excitation energy is absorbed predominantly by the heavy fragment, leading to $\Delta\nu_H \simeq 0.5$. This corresponds closely to the total increase in excitation energy of 4.7 MeV.

The correlation between total kinetic energy and the number of prompt fission neutrons is another important feature for the understanding of the fission mechanism. The total kinetic energy mainly arises from Coulomb repulsion, which depends on fragment deformation at the scission point. On the other hand, the deformation energy contributes to the internal fragment excitation characterized by the number of evaporated fission neutrons. Therefore, the distribution of $\nu(\mathrm{TKE}^*)$ may help to investigate whether the interplay between deformation energy and

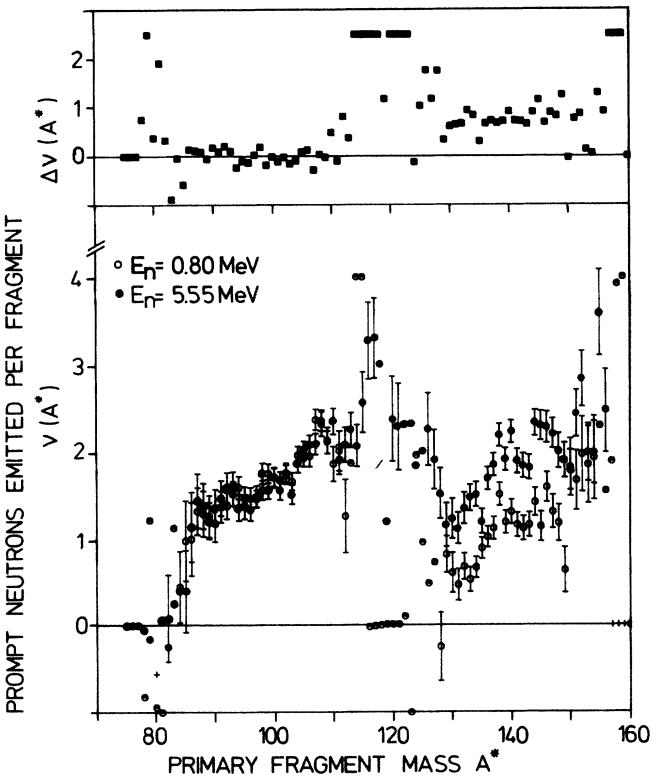

FIG. 6. Average number of prompt neutrons ν_{tot} vs primary fragment mass for $E_n=0.8$ and 5.5 MeV.

internal fragment excitation energy accounts for the observed effects or whether other mechanisms, e.g., fission dynamics, need to be considered. Figure 7 shows the distribution of ν(TKE*) for $E_n=5.5$ MeV. In order to improve statistics, the data have been integrated from mass 133 to 143. One finds that ν(TKE*) decreases linearly with total kinetic energy with a gradient of -0.11 MeV^{-1}. This is an interesting result because it confirms the estimated 8 MeV excitation energy required for evaporation of a neutron, and this, in turn, supports the quasistatic fission model of Wilkins, Steinberg, and Chasman:[9] Significant dynamical effects would tend to destroy, or at least disturb, the correlation between ν and TKE* (also see Sec. IV).

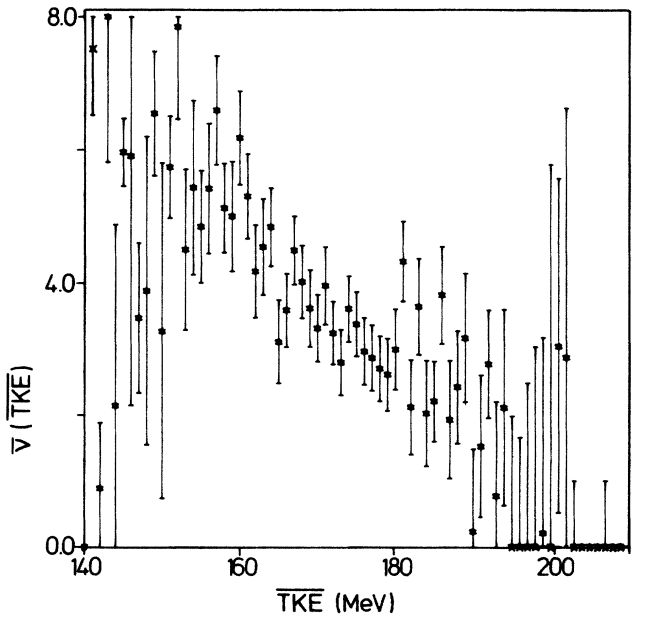

FIG. 7. Number of prompt fission neutrons as a function of total kinetic energy (integrated over the mass region 111–143) for $E_n=5.5$ MeV.

E. Variances and mean values

Not only the distributions of total kinetic energy, TKE(A^*), and prompt neutrons, $\nu(A^*)$, but also their variances σ, are important parameters to describe the fission fragment properties. Because of the strong correlation between $E_{k,\mathrm{tot}}$ and fragment deformation, the variance $\sigma_{E_{k,\mathrm{tot}}}$ provides a hint for the variance of fragment deformation at the scission point. In Fig. 8 the variance of the total kinetic energy is plotted as a function of fragment mass for $E_n=0.8$ and 5.5 MeV. Note the apparent change in the distribution at $A^*\simeq 138$, which is consistent with the model prediction of Wilkins, Steinberg, and Chasman[9] (see Sec. IV B).

The mean values of all relevant quantities are summarized in Table II. For comparison or for illustration of systematic trends, we have also included the results of the $(2E,2v)$ experiment of Andritsopoulos,[7] which were obtained for ^{235}U at thermal neutron energies.

IV. DISCUSSION

In the following, the results of this experiment will be compared with the quasistatic model of Wilkins, Steinberg, and Chasman.[9] Qualitatively, this model provides a satisfactory description of fission fragment properties in the region of Po to Fm. At the scission point, the fissioning system is described by two coaxial spheroids with

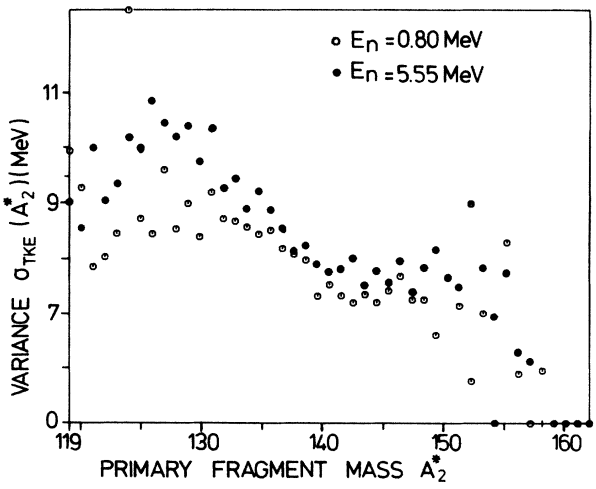

FIG. 8. Variance of the total kinetic energy as a function of heavy fragment mass for $E_n=0.8$ and 5.5 MeV.

TABLE II. Mean values of fragment properties for fission of ^{237}Np at 0.8 and 5.55 MeV neutron energy. For comparison the results of Andritsopoulos (Ref. 7) are included. The quoted errors are statistical uncertainties only.

		^{235}U(n_{th},f)	^{237}Np(n,f) This work	
		Andritsopoulos	E_n=0.5 MeV	E_n=5.5 MeV
Saddle point excitation (MeV)		0.8	0.1	4.8
Primary fragment mass	A_L^*	95.87±0.07	98.66±0.06	99.12±0.05
Variance	$\sigma_{A_L^*}$	6.3	5.80±0.05	6.59±0.05
Secondary fragment mass	A_L	94.71±0.06	97.07±0.06	97.53±0.06
	A_H	138.60±0.06	138.21±0.06	137.01±0.06
Variance	σ_{A_L}	5.7	5.60±0.07	6.33±0.07
	σ_{A_H}	5.7	5.59±0.07	3.36±0.09
Fragment velocities (cm/ns)	v_L	1.415	1.3997±0.0013	1.3893±0.0013
	v_H	0.97	0.9874±0.0010	0.9877±0.0009
Variance	σ_{v_L}	0.051	0.0591±0.0009	0.0738±0.0008
	σ_{v_H}	0.086	0.0742±0.0007	0.0782±0.0006
Total kinetic energy (MeV)	$E^*_{k,\mathrm{tot}}$	167.45±0.07	174.80±0.37	173.53±0.35
	$\sigma_{E^*_{k,\mathrm{tot}}}$	14.2	10.39±0.09	10.43±0.08
Number of neutrons	ν_L	1.16±0.09	1.59[a]	1.59±0.08
emitted per fragment	ν_H	1.27±0.09	1.14[a]	1.87±0.08
	$\Delta\nu_L/\Delta A^*$		0.046±0.005	0.048±0.005
	$\Delta\nu_H/\Delta A^*$		0.046±0.007	0.043±0.008
Peak-to-valley ratio	P/V		650±125	31±3
Gradient with excitation energy	$\Delta E_{k,\mathrm{tot}}/\Delta E_{\mathrm{exc}}$		−0.27±0.11	

[a]Results of this work combined with radiochemical data. The respective uncertainties include the normalization.

quadrupole deformations which are characterized by three parameters. These three parameters are the distance d between the surfaces of the spheroids and the temperatures τ_{int} and T_{coll}, associated with the internal and collective degrees of freedom. The crucial assumption is that the fragment distributions at the scission point can be determined from the relative potential energies of the nascent fragments. These energies are calculated from the fragment deformations β_i and their neutron and proton numbers N and Z. The potential energy is given by

$$V=\sum_i (V_{\mathrm{LD}i}+S_i+P_i)+V_C+V_n,\quad i=1,2\ .$$

The main contribution comes from the liquid drop term $V_{\mathrm{LD}i}$. The shell corrections S_i have been made using the Strutinsky method, while the pairing corrections P_i were calculated with the usual BCS formalism. V_C and V_n account for the Coulomb repulsion and the final nuclear interaction of the two fragments at distance d. For the internal excitation a constant value $\tau_{\mathrm{int}}=0.75$ MeV was chosen, corresponding to a partial coupling between single particle degrees of freedom and collective degrees of freedom, instead of a pure adiabatic approximation with $\tau_{\mathrm{int}}=0$. The collective degrees of freedom are assumed to be strongly coupled and to be in partial statistical equilibrium, characterized by the temperature T_{coll}. The relative probability P of different fragmentation then follows from

$$P=\int_{\beta_1}\int_{\beta_2}\exp|-V/T_{\mathrm{coll}}|\,d\beta_1 d\beta_2\ .$$

The model shows that neutron shell corrections play a dominant role, whereas proton shell corrections and neutron and proton pairing corrections are of minor importance. The shell corrections of Ref. 9 are presented in Fig. 9, because they are subsequently referred to. However, quantitative analyses are difficult to obtain with this model due to the sizeable uncertainties in the shell corrections.

A. Mass distribution and mass asymmetry

The preference for asymmetric mass division for ^{237}Np is easily understood from the behavior of neutron shell corrections. There is no pronounced minimum of the shell correction for symmetric fission (N=72,73), while asymmetric pairs have minima at either F and G or H

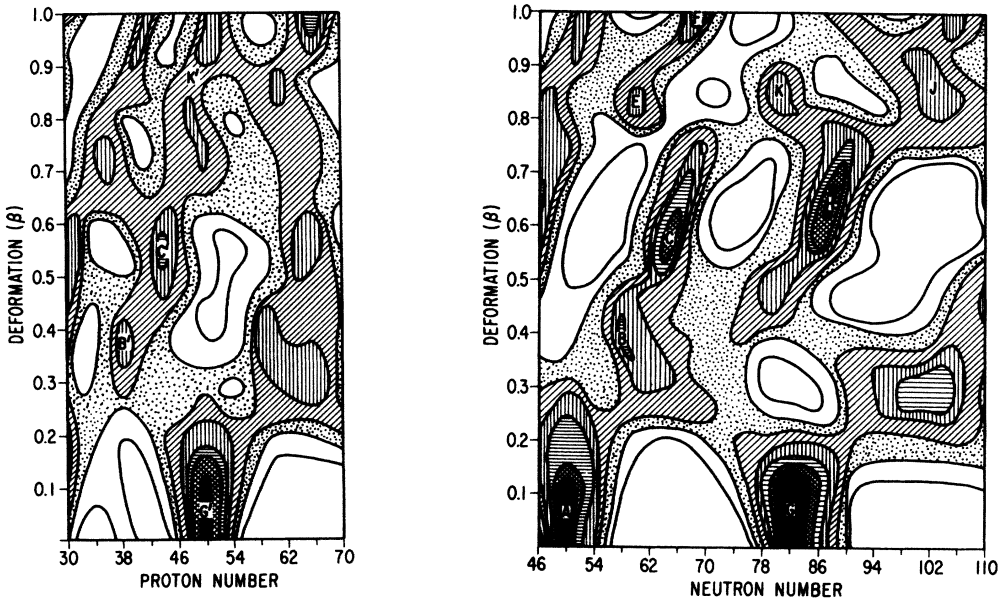

FIG. 9. Shell corrections to the potential energy for neutrons and protons. The figure is taken from the work of Wilkins, Steinberg, and Chasman (Ref. 9). Contours are plotted in intervals of 1 MeV with the black regions containing all values lower than -4 MeV and the inner white regions containing all values greater than $+2$ MeV. The letters refer to particular shell regions as described in the text.

and C. The LDM energy on which the shell corrections are superimposed favors deformations around $\beta=0.6$; therefore, the division H,C is energetically preferred. Consequently, doubly magic fragments near the minima at G and G' with $A\simeq 132$ occur relatively seldom. The increase in symmetric fission with excitation energy suggests that the influence of shell effects (which are also of the order of 5 MeV) is correspondingly weaker. Comparison of the experimental and calculated fragment mass distribution shows that the calculated distribution is too narrow. This discrepancy could be resolved if the shell correction for the light fragment between regions A and B in Fig. 9 were reduced by approximately 2 MeV.

As Wilkins *et al.*[9] did not treat ^{237}Np explicitly, the fine structure of the mass distribution cannot be compared with theory. If one therefore restricts the comparison to the experimental data for ^{235}U (Ref. 1), one finds that the fine structure in ^{237}Np has twice the period but only half the intensity compared to ^{235}U. In the division of the odd-odd nucleus ^{238}Np into two fragments, there is always an unpaired neutron and proton. Hence, there should be no preference for certain mass splits due to the pairing effect. According to Ashgar *et al.*,[3] the observed fine structure in the case of ^{237}Np might therefore rather be due to shell effects in the deformed fragments than in the fissioning system.

B. Kinetic energy distribution

The trend of the total kinetic energy distribution and its variance can be explained qualitatively by the model of Wilkins *et al.* The distance between the charge centers of both fragments is approximated by the sum of the fragment deformations $\beta=\beta_1+\beta_2$. As shell effects are weak for a symmetric mass split, the flat minimum in the potential energy which results from the LDM part for $\beta_1 \simeq\beta_2\simeq 0.65$ determines the fragment shape around $A=118$. This relatively large deformation leads to a large distance between the fragments and hence to a reduction of the total kinetic energy, as is observed experimentally.

With increasing asymmetry, one finds from Fig. 9 a very small deformation for the doubly magic fragment at $A=132$ (at minimum G), whereas the complementary fragment has a large deformation (minima E or F). The resulting total deformation $\beta\simeq 1.0$ is significantly smaller than for symmetric fission, leading to the maximum in total kinetic energy around mass 132. As the mass split becomes more asymmetric, the heavy fragment deformation increases to $\beta_2=0.6$–0.7 (region H in Fig. 9) and β_1 moves from C to A via B. For these fragment pairs the total deformation lies between 1 and 1.2 and hence the total kinetic energy decreases again. This trend is enhanced because of the decreasing product (Z_1Z_2) for $A>130$.

Besides the qualitative understanding of $E^*_{k,\mathrm{tot}}(A^*)$, the model of Wilkins *et al.* provides also an explanation for the variance $\sigma_{E_{k,\mathrm{tot}}}$ around $A\simeq 140$. For fragments of mass number $A=138$ and neutron number $N=84$, the complementary fragments have $N=61$ neutrons. While the deformation of the heavy fragment is fixed by the deep minimum H in Fig. 9, there is no preference for a specific deformation of the light fragment in the broad region between B and C. Hence, the respective deformations β_1 scatter significantly, resulting in a large variance of the kinetic energy. For heavy fragment masses beyond $A=140$, the deformation of the light fragment is confined to the region near B and thus the variance $\sigma_{E_{k,\mathrm{tot}}}$ decreases.

We find, that the Wilkins *et al.* model is compatible with the experiment in all aspects concerning $E_{k,\mathrm{tot}}$. The observations can be explained by means of fragment deformation at the scission point. A significant effect of prescission kinetic energy could not be identified.

C. Prompt fission neutrons

While the total kinetic energy is an indicator for fragment deformation, the number of prompt fission neutrons provides a measure of internal fragment excitation. The internal excitation energy of the fragments E_{exc} is composed of the deformation energy and of the internal excitation energy which the fragments gain between saddle and scission point due to the (perhaps weak) coupling between collective and particle degrees of freedom. The comparison with the model of Wilkins *et al.* confirms for a symmetric mass split the expected large number of prompt fission neutrons due to the large fragment deformations. For the magic heavy fragments, i.e., for $A=132$ around the minimum G, the number of prompt neutrons is practically zero and increases rapidly with increasing mass asymmetry. Correspondingly, the number of prompt neutrons emitted from the light fragments decreases with increasing mass asymmetry as its deformation moves from the minimum D to A via C and B. Quantitatively, the sawtooth curve predicted by the model is too low for the light fragments and too high for heavy fragments.

Another problem arises with respect to the predicted change of $\nu(A^*)$ with excitation energy. From the deep minimum H in Fig. 9 one would expect that shell effects should be more pronounced for the heavy fragments. Therefore, it is very surprising that apparently all of the extra excitation energy at 5.5 MeV shows up in the heavy fragment and none in the light.

In spite of this inconsistency, the trend of $\nu(A^*)$ is in reasonable agreement with the predictions of the model. Apparently, the weak coupling between collective and single particle degrees of freedom is justified, because otherwise the correlation between fragment deformation and $\nu(A^*)$ would be significantly disturbed.

V. CONCLUSIONS

A comparison of the results for ^{237}Np with the model calculation of Wilkins *et al.*[9] confirms our earlier conclusions obtained for ^{235}U: The model allows for a qualitative explanation of the experimental facts, but some more specific results, such as the mass and energy dependence of $\nu(A^*)$, indicate that the model requires some modifications concerning the shell effects of heavy fragments.

In particular, we found no strong differences in fragment properties for the two fissioning systems, the odd-odd ^{238}Np and the even-even ^{236}U (besides the fine structure of the mass distribution). This suggests, that pairing effects—although important in the fission mass distribution—do not appear to have an observable effect on other fragment properties.

ACKNOWLEDGMENTS

We thank Professor G. Schatz and Professor F. Gönnenwein for their continuous interest and support. We appreciate the excellent sample preparation at the University of Munich by Dr. H. J. Maier, the careful technical assistance of G. Rupp, and the important contribution of A. Ernst and D. Roller from the Van de Graaff team in providing the computer controlled fast pulsed proton beam. This work was carried out at Kernforschungszentrum Karlsruhe and was supported, in part, by the Bundesministerium für Forschung und Technologie.

---

*Present address: University of Petroleum and Minerals, Department of Physics, Dhahran, Kingdom of Saudi Arabia.

†Present address: Siemens AG, D-8000 München, Federal Republic of Germany.

[1]R. Müller, A. A. Naqvi, F. Käppeler, and F. Dickmann, Phys. Rev. C **29**, 885 (1984).

[2]B. D. Kuzminov, A. I. Sergachev, and L. D. Smirenkina, Yad. Fiz. **11**, 297 (1970) [Sov. J. Nucl. Phys. **11**, 166 (1970)].

[3]M. Ashgar, P. D'Hondt, C. Guet, P. Perrin, and C. Wagemans, Nucl. Phys. **A292**, 225 (1977).

[4]A. A. Naqvi, Report No. KfK-2919, Kernforschungszentrum Karlsruhe (1980).

[5]H. W. Schmitt and F. Pleasonton, Nucl. Instrum. Methods **40**, 204 (1966).

[6]R. Müller, A. A. Naqvi, F. Käppeler, and Z. Y. Bao, Report No. KfK-3220, Kernforschungszentrum Karlsruhe (1981).

[7]G. Andritsopoulos, Nucl. Phys. **A94**, 537 (1967).

[8]J. P. Unik, J. E. Gindler, E. Glendenin, K. F. Flynn, A. Gorski, and R. K. Sjobl, in *Physics and Chemistry of Fission 1973* (IAEA, Vienna, 1974), Vol. 2, p. 19.

[9]B. D. Wilkins, E. P. Steinberg, and R. R. Chasman, Phys. Rev. C **14**, 1832 (1976).

[10]N. I. Borisova, V. I. Novgorodtseva, V. A. Pchelin, and V. A. Shigin, Yad. Fiz. **2**, 243 (1965) [Sov. J. Nucl. Phys. **2**, 173 (1966)].

[11]L. R. Veeser, Phys. Rev. C **17**, 385 (1978).

[12]J. Fréhaut, A. Bertin, and R. Bois, in *Nuclear Data for Science and Technology*, edited by K. H. Böckhoff (Reidel, Dordrecht, 1983), p. 78.